Discrete superconducting phases in proton-intercalated FeSe thin flakes

W. X. Wang,[1] B. Lei,[1] C. S. Zhu,[1] J. H. Cui,[1] W. Z. Zhuo,[1] Z. J. Xiang,[1] X. G. Luo,[1] and X. H. Chen[1,2,3,*]

[1]*Department of Physics, University of Science and Technology of China, and Key Laboratory of Strongly Coupled Quantum Matter Physics, Chinese Academy of Sciences, Hefei 230026, China*

[2]*CAS Center for Excellence in Superconducting Electronics (CENSE), Shanghai 200050, China*

[3]*CAS Center for Excellence in Quantum Information and Quantum Physics, Hefei, Anhui 230026, China*

(Received 10 March 2022; revised 14 June 2022; accepted 29 June 2022; published 13 July 2022)

We have successfully manipulated the electronic properties of FeSe thin flakes based on a field-effect transistor with a solid proton conductor as the gate dielectric. The phase diagram as a function of gate voltage demonstrates three evident discrete superconducting phases with T_c corresponding to ∼8, ∼34, and ∼42 K, respectively, which is similar to those observed in Li_xFeSe and Na_xFeSe by tuning Li or Na content with the solid-ion-conductor gating technique. In the protonation process, the final state with a saturation of the amount of hydrogen ions is reached at a moderately low gate voltage. It suggests that such a device based on a proton conductor can be used to modulate the physical properties by controlling the intercalated proton content and to explore the hydrogen storage capacity of materials.

DOI: 10.1103/PhysRevB.106.014509

I. INTRODUCTION

Iron selenide, with the simplest crystal structure among iron-based superconductors, is thought to be an ideal platform to study the basic physics of the iron-based superconducting family, which has attracted great interest. Its superconducting transition temperature ($T_c \approx 8$ K) can be significantly enhanced to 36.7 K under an external pressure [1]. Signs of even an enhancement of T_c up to 65 K in a monolayer FeSe film grown on $SrTiO_3$ have been observed [2–4]. This high-T_c superconductivity is possibly due to electron-phonon coupling and charge transfer through the interface. In addition, electron doping is capable of largely enhancing T_c as well. Alkali-metal-intercalated FeSe superconductors, $A_xFe_{2-y}Se_2$ (A = K, Rb, and Cs), have a T_c of around 32 K [5–7]. The intercalation of alkali metals would dope electrons into FeSe layers, but there are plenty of Fe vacancies in the FeSe layer. A T_c as high as 43 K was observed in an $(Li_{0.8}Fe_{0.2})$OHFeSe superconductor [8]. The $(Li_{0.8}Fe_{0.2})$OH layer is the charge reservoir block, and the transfer of electrons to the FeSe layer could be the main reason for the high-T_c superconductivity in this system. Furthermore, organic-ion-intercalated FeSe superconductors synthesized by an electrochemical method have a T_c of more than 40 K [9,10]. The enhanced T_c should originate from the charge transfer of electrons into the FeSe plane. The huge distance between adjacent FeSe layers caused by organic-ion intercalation renders these systems strongly anisotropic [11].

Tuning the carrier concentration by a gating technique can manipulate the physical properties of materials more precisely than chemical doping. It provides an effective way to induce high-T_c superconductivity [12]. An achievement of a high-T_c phase from a low-T_c phase through electrostatic gating by using an ionic liquid as the gate dielectric was reported in a previous work of gating for FeSe thin flakes [13]. However, the doping level is limited due to sample damage at a high gate voltage. The solid-state ionic gating technique is also successfully applied to tuning the phase transition in FeSe thin flakes [14,15]. A series of discrete superconducting phases have been observed in the process of intercalating Li and Na ions [15], which is clearly distinct from all other observations on unconventional superconductors. It was reported that the intercalation of Li^+ would change the crystal structure of the sample, lead the sample into an irreversible state [16], and even damage the sample at higher doping levels. Compared with gates of solid lithium/sodium ionic conductors, protonic gates are more reversible and controllable, mainly because of the smaller size of the protons. It is more widely applied [17–21]. Recently, hydrogen ions produced from electrolyzed water by ionic liquid gating were diffused into iron-based superconductors, leading to an enhancement of T_c [17]. Such a device always works at room temperature or even higher [21]. Another route of tuning the proton concentration based on a field-effect transistor with a solid proton conductor as the gate dielectric can be used at temperatures well below room temperature, and the content of protons can be controlled by gating voltage, which is totally different from the diffusion of protons produced by electrolyzed water [19,20]. Therefore, it will benefit for manipulating the properties of materials. Meanwhile, the exposed surface of the sample in the device makes it possible to perform some *in situ* characterization as well as the construction of a heterostructure or interface engineering, in contrast to the former technique where the sample is covered by ionic liquid.

In this paper, we modulate the electronic properties of FeSe thin flakes by using a proton-conductor-based field-effect transistor and map out the phase diagram as a function of

*chenxh@ustc.edu.cn

gate voltage. In this protonation process, we find three discrete superconducting phases in the phase diagram, similar to those observed by intercalating Li^+/Na^+ into FeSe in previous work [12]. Starting from a $T_c = 8$ K phase, two superconducting phases with $T_c = 34$ and 42 K are successively observed with increasing gate voltage. The resistance and Hall coefficient no longer change upon further gating after achieving the optimal doping level ($T_c = 42$ K, at $V_g = 12.6$ V), strikingly distinct from Li_xFeSe and Na_xFeSe [12] in which the superconducting to insulating phase transition is accompanied by a structural transition due to Li intercalation. It indicates that the hydrogen content in our FeSe flake becomes saturated as the gate voltage is over 12.6 V. Hall measurement reveals the enhanced T_c is closely related to the electron doping.

II. EXPERIMENT

We use porous silica films as proton conductors deposited on a conductive Nb-doped $SrTiO_3$ substrate (any other conductive substrate can be used). The porous silica is prepared by a sol-gel process [22]. After mixing tetraethyl orthosilicate, ethanol, water, and phosphoric acid (as a proton source, 85 wt %) in a molar ratio of 1 : 18 : 6 : 0.03 in a sealed bottle, we stirred it for 2 h and then annealed it at 60 °C for another 2 h. Afterward, the solution was spin coated onto the substrate at 3000 rpm for 30 s and baked at 150 °C for 25 min. To reduce the gate drain current through the porous silica, the spin coating and baking steps were performed once again for increasing the thickness of the proton conductor to about 450 nm (see Fig. S1 in the Supplemental Material [23]). FeSe thin flakes were mechanically exfoliated from a high-quality single crystal and then transferred onto the proton conductor films by using a piece of transparent polydimethylsiloxane (PDMS) film. The thickness of the flakes was characterized by atom force microscopy (AFM). Then Cr/Au (5/50 nm) were deposited on the samples as electrodes in a standard Hall bar configuration. The transport properties of the device were carried out in a commercial Quantum Design physical property measurement system (PPMS).

III. RESULTS AND DISCUSSIONS

Figure 1(a) shows the configuration of the electrically gated device placed on a solid proton electrolyte. A single-crystalline FeSe thin flake with a typical thickness of 18 nm [shown in Fig. 1(d)] serves as the transport channel. Figure 1(b) shows an optical image of the device. To reduce the gate leakage current, the gate voltage is applied at 190 K, where all the hydrogen ions in the electrolyte are frozen (see Fig. S2 [23]). With slowly heating to 220 K at a rate of 1 K/min, protons are driven into the sample by the electric field. Then, it was held at 220 K for 1 min before cooling down rapidly to a low temperature.

As protons enter into FeSe, the resistance of the sample decreases. Figure 2(a) presents the detailed evolution of resistance with increasing gate voltage. As shown in Fig. 2(a), there exist a series of discrete superconducting transitions in the proton-intercalated FeSe, which seems analogous to that observed in intercalating Li^+/Na^+ into FeSe [15]. At

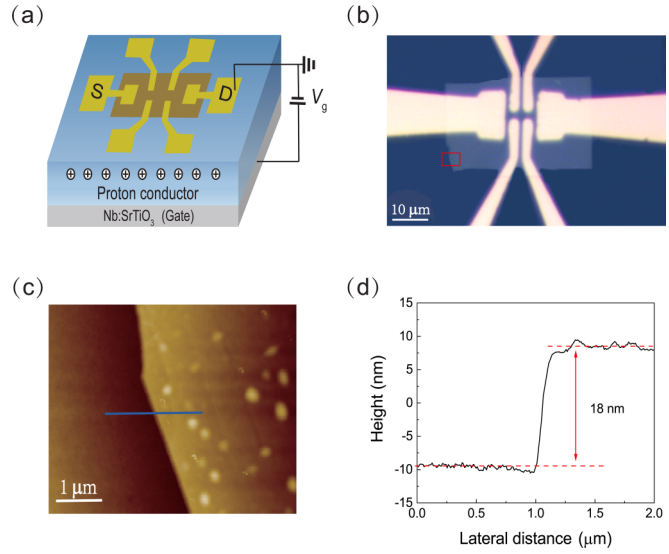

FIG. 1. (a) Schematic structure of the solid proton conductor gating device. From the bottom to the top: Nb-doped $SrTiO_3$ substrate (as the gate electrode), 300-nm-thick porous silica (as the proton conductor), FeSe thin flake, and electrodes with a standard Hall bar configuration. (b) An optical image of the device. Scale bar: 10 μm. (c) An AFM image of the enlarged view of the portion enclosed by the red rectangle shown in (b). Scale bar: 1 μm. (d) The thickness of the flake from the step height is determined to be 18 nm.

$V_g = 0$ V, the sample is superconducting with an onset critical temperature $T_c^{onset} = 7.3$ K, as demonstrated in Fig. 2(c). As the applied gate voltage is raised to $V_g = 8.4$ V, the T_c (in this paper we use T_c^{onset} as T_c) is still around $T_{c1} = 8$ K (T_c of a bulk FeSe single crystal). A superconducting transition $T_{c2} \approx 34$ K abruptly appears with continuously enhancing V_g up to 8.53 V,

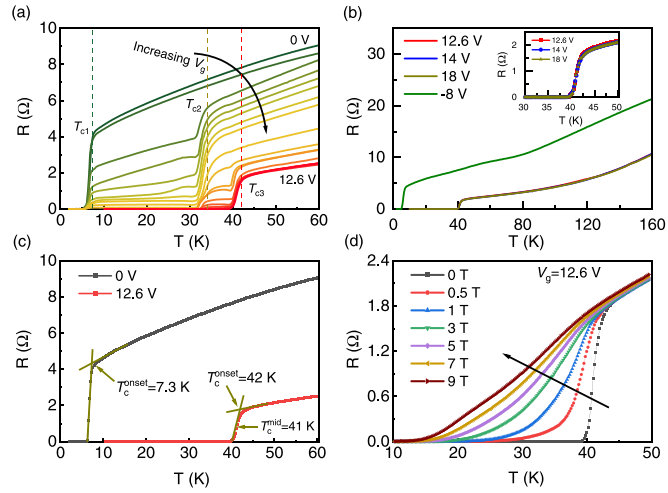

FIG. 2. Temperature dependence of resistance taken at various gate voltages. (a) Resistance under the gate voltage from 0 to 12.6 V. (b) Resistance at the gating voltage from 12.6 to 18 V, and at $V_g = -8$ V. The inset is the magnified view of the region near the superconducting transition at the gating voltage from 12.6 to 18 V. (c) Resistance at the initial and optimal superconducting state. (d) Resistance near the superconducting transition under the perpendicular magnetic field up to 9 T and at $V_g = 12.6$ V.

which initially coexists with T_{c1}. Thereafter, T_{c2} is maintained at 34 K, but this superconducting transition becomes sharper and sharper, and the T_{c1} phase progressively fades away. Upon further increasing V_g up to 9.5 V, the superconducting transition at T_{c1} vanishes. Meanwhile, another superconducting transition with $T_{c3} = 42$ K emerges, coexisting with the T_{c2} phase. With further improving V_g, the T_{c3} phase remains, accompanying the suppression of the T_{c2} phase (it vanishes as V_g increases to about 10.9 V). Eventually, the optimal superconductivity of the FeSe thin flake with a midpoint critical temperature $T_c^{mid} = 41$ K and a zero-resistance state below 39 K [see Fig. 2(c)] was obtained at $V_g = 12.6$ V. As shown in Fig. S3, the high-T_c phase in ionic-liquid-gated FeSe has a superconducting transition width as high as a dozen degrees Kelvin, whereas in our case the superconducting transition width is only 3 K at the optimal superconducting state [23]. The sharp transition suggests that the charge doping and enhanced superconductivity should be a bulk effect and originate from proton intercalation.

In previous work, the magnetic susceptibility measurement shows that the T_c of a protonated bulk FeSe single crystal was enhanced to 41 K under an optimized gating condition (using an ionic liquid gate and applying a gate voltage of $V_g = 3$ V at 350 K for 12 days) [21]. The result is consistent with the T_c for the optimally doped state in our work. However, our work, using the solid-state proton conductor gating technique, can achieve an optimally superconducting phase much more conveniently and rapidly. In Fig. 2(d), the variation of $R(T)$ near T_c is plotted against the perpendicular magnetic field for the optimally superconducting state. The width of the superconducting transition increases significantly upon applying magnetic fields, but the onset superconducting transition temperature drops very little.

FeSe with proton intercalation ultimately does not enter into an insulating state, which is different from Li_xFeSe and Na_xFeSe [15]. Resistance shows no further change as the gating voltage exceeds 12.6 V, as illustrated in Fig. 2(b). As shown in the bottom inset of Fig. 3, there is hardly any variation in Hall resistance at 50 K as the gate voltage exceeds 12.6 V. When the sample reaches an optimally superconducting state, the concentration of hydrogen ions in FeSe cannot be enhanced any more with further increasing the gating voltage. It does not result from an insufficient hydrogen ion content in the proton conductor. In fact, the content of hydrogen ions in the proton conductor film was approximately $\sim 10^{-9}$ mol. The amounts of Fe atoms in our FeSe thin flakes were approximately $\sim 10^{-12}$ mol, which is much smaller than that of hydrogen ions in the proton conductor film. Hence, the amount of protons is completely sufficient for the sample. When the sample reaches the optimal superconducting state, there is still a large amount of hydrogen remaining in the proton conductor. In addition, for another 18-nm-thick FeSe flake, we used a thicker proton conductor with a thickness of about 670 nm that accommodates more hydrogen ions to modulate its electronic properties (see Fig. S5 [23]). It also eventually entered the optimal superconducting state with the same T_c and did not change with continuously increasing gate voltage. It suggests that the hydrogen content in the FeSe flake becomes saturated as the gate voltage exceeds 12.6 V. It should be addressed that the evolution procedure from the

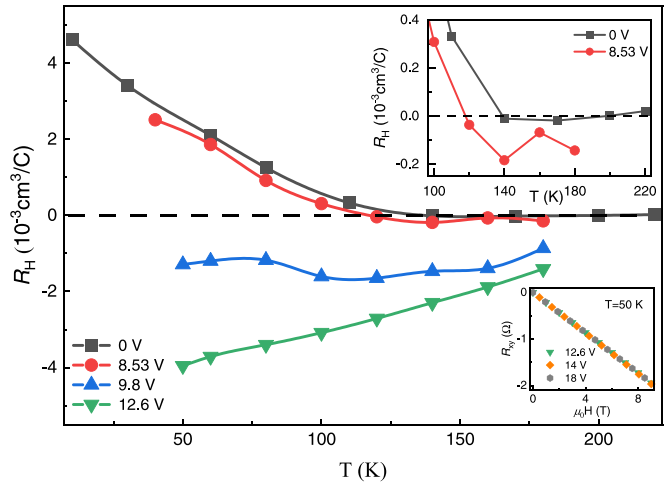

FIG. 3. Temperature dependence of the Hall coefficient R_H, calculated from the linear fit of a $R_{xy}(B)$ plot from −9 to 9 T. For the nonlinear $R_{xy}(B)$ curves, we extract R_H from the slope of the high-field quasilinear part. The four typical gate voltages correspond to four different states of the sample, which are initial, coexisting T_{c2} and T_{c1}, coexisting T_{c3} and T_{c2}, and optimal superconducting state, respectively. An enlarged view of $R_H(T)$ from 100 to 220 K at $V_g = 0$ and 8.53 V is illustrated in the top right center. The inset in the bottom right is the magnetic field dependence of Hall resistance R_{xy} at the gating voltage from 12.6 to 18 V and at 50 K.

T_{c1} to T_{c3} phase is partially reversible, as the T_{c1} phase can be restored by sweeping V_g from 12.6 to −8 V.

Concerning why the situations are different upon further gating after achieving optimal doping in H^+/Li^+-intercalated FeSe, the weaker chemical activity of hydrogen ions compared to Li^+ and Na^+ ions might be taken into account. With further increasing the concentration of Li^+ after achieving optimal doping, the crystal structure of the sample changes, and the sample reaches an irreversible insulating state [14–16]. while the positions of x-ray diffraction (XRD) peaks (comparing between $FeSe_{0.93}S_{0.07}$ and $H_xFeSe_{0.93}S_{0.07}$, FeS and H_xFeS, $BaFe_2As_2$, and $H_xBaFe_2As_2$) do not show a discernible change after protonation in a previous report [18], which represents that the original crystal structures of the corresponding materials can be kept with proton intercalation. The same situation occurs in organic-ion-intercalated FeSe synthesized by the electrochemical method. When the optimal doping level is reached through the intercalation of organic ions, such as $(CTA)_{0.3}FeSe$ [10] and $(TBA)_{0.3}FeSe$ [11], extending the chemical reaction time cannot lead to a higher doping concentration. In our case, when the optimal superconducting state is achieved, no more excess hydrogen ions can enter into the sample. Our studies demonstrate that such proton-conductor-based devices may be used to explore the hydrogen storage capacity of materials.

To further reveal the evolution of the electronic properties in the protonation process, we studied the Hall resistance R_{xy} of an FeSe thin flake under four typical gate voltages, which correspond to different superconducting states. The temperature dependence of the Hall coefficient R_H is summarized in Fig. 3. A gradual decrease of R_H with intercalating protons indicates that electrons are doped into FeSe in this gating

process. In the initial state ($V_g = 0$ V, T_{c1} phase), $R_H(T)$ has a similar overall behavior to that in the bulk FeSe as reported previously [20]. The sign of R_H has changed twice from positive to negative, and back to positive at low temperature when the sample is cooled from high temperature to 2 K, indicating the multiple band system. At $V_g = 8.53$ V (coexisting superconducting phases of T_{c2} and T_{c1}), the temperature dependence of R_H retains a majority of features, but the sign of R_H changes from negative to positive in the cooling process.

Unfortunately, we cannot get the sample which shows superconductivity with only a T_{c2} transition in resistivity, probably due to the inhomogeneous distribution of H^+ or metastability of the T_{c2} superconducting phase. With increasing V_g to 9.8 V, both of the 34 and 42 K phases coexist in the sample. The $R_H(T)$ is strikingly different from the case discussed at the two voltages of 0 and 8.53 V. The R_H is negative in the entire temperature range for measurement. When the gating voltage rises to 12.6 V, the optimally superconducting state with the T_{c3} phase is achieved. The R_H remains negative and decreases gradually with decreasing temperature. A similar $R_H(T)$ has been observed in the ionic-liquid-gate-induced high-T_c phase of FeSe [13] and an optimally doped (Li,Fe)OHFeSe flake with $T_c = 43.4$ K [24].

As the gating voltage exceeds 12.6 V, the Hall resistance measured at 50 K shows no further changes, which is consistent with the result of the resistance measurement. In the previous works, the achieved maximum electron doping level enhances the T_c to 48 K, and further gating leads to damaging the device due to the electrochemical reaction for the ionic liquid gating in FeSe thin flakes [13]. Also, a solid Li-ion conductor as the gate dielectric can bring a higher electron doping concentration for FeSe thin flakes, while the excessive Li ions driven into the sample change the crystal structure, accompanied by a phase transition from a superconducting to insulating state [14]. It suggests that further electron doping makes it possible to achieve a higher transition temperature in FeSe without destroying the sample. It is unfortunate that when the sample reaches the optimal superconducting state, the concentration of hydrogen ions in the sample also reaches saturation and can no longer deliver more carriers in our case.

Previous studies on FeSe confirm that its Fermi surface consists of both hole and electron pockets [25,26]. However, only electron pockets can be observed in all of the FeSe-derived superconductors with T_c above 30 K, for instance, $K_xFe_{2-y}Se_2$ [27], $(Li_{0.8}Fe_{0.2})$OHFeSe [28], and the monolayer FeSe film grown on $SrTiO_3$ [3,4]. With the electron doping, the hole pockets disappear with an E_F shift to a certain energy, leveling the Fermi surface with only electron pockets. There exists a sudden change in the Fermi surface topology, and the so-called Lifshitz transition occurs. The evolution from a low-T_c to high-T_c phase has been observed around the Lifshitz transition in ionic-liquid-gated FeSe [13]. A clear evolution of the Fermi surface topology has been observed in surface K-dosed FeSe films by angle-resolved photoemission spectroscopy (ARPES) [29]. In our case, in contrast to that observed at $V_g = 0$ V, R_H taken at $V_g = 12.6$ V is negative in the whole measurement temperature range. The dramatic change in R_H with increasing gate voltage indicates a possible Lifshitz transition when the system evolves from the T_{c1} to T_{c3} phase. The step of the T_c increase from 8 to 34 K could be either due to a Lifshitz transition or a sudden modification in the pairing strength in terms of related reports of theoretical mechanisms [30,31].

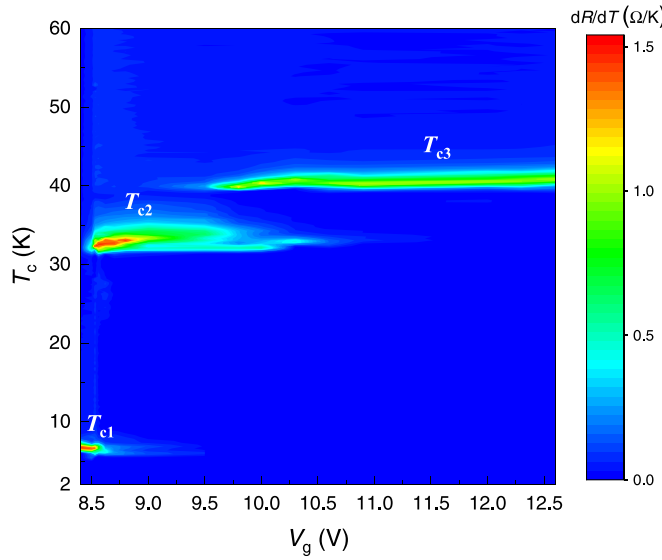

FIG. 4. The phase diagram of a proton-intercalated FeSe thin flake as a function of gate voltage. Color contour plots of derivatives of the $R(T)$ curves in Fig. 2(a).

Based on the resistance measurements, the phase diagram of the H^+-intercalated FeSe thin flake is plotted as a function of gate voltage in Fig. 4. The color scale represents the amplitude of dR/dT [i.e., the derivative of $R(T)$ curves shown in Fig. 2(a)]. Three discrete superconducting phases in proton-intercalated FeSe are clearly seen. Pristine samples and those with a small amount of H^+-doped states exhibit a T_{c1} phase. With increasing V_g up to 8.5 V, the T_{c2} phase appears. Upon further increasing V_g, the T_{c3} phase emerges. Optimal superconductivity is achieved at $V_g = 12.6$ V, and further increasing the gate voltage cannot alter the resistance any more and the T_{c3} remains the same until the sample is damaged. We mention that V_g may not be an ideal independent variable for mapping the phase diagram, since the proton doping is a cumulative process and keeping a fixed gate voltage with a prolonged time can access different states as well. For the data shown in Fig. 4, we used a constant relaxation time (1 min) for each gate voltage and a constant cooling rate for the measurement of $R(T)$, so in this sense, V_g reflects the actual doping concentration and thus can serve as an independent variable for tracing the chemical states of our sample.

IV. CONCLUSION

We have successfully manipulated the electronic properties of FeSe thin flakes by a protonic gate and mapped out a phase diagram as a function of gate voltage. Three evident discrete superconducting phases are observed, similar to those reported previously in Li_xFeSe and Na_xFeSe. The enhanced T_c is closely related to the electron doping as revealed by the Hall measurement, and enhanced to 42 K at an optimal gating condition. The resistance and Hall coefficient do not vary with further increasing gating voltage, once the optimal

doping level is achieved. It suggests that such devices based on the proton conductor can be used to modulate the physical properties and to explore the hydrogen storage capacity of materials.

ACKNOWLEDGMENTS

This work was supported by the National Natural Science Foundation of China (11888101, 11534010, and 12004365), Anhui Initiative in Quantum Information Technologies (AHY160000), the National Key Research and Development Program of the Ministry of Science and Technology of China (2017YFA0303001 and 2019YFA0704901), the Science Challenge Project of China (Grant No. TZ2016004), the Key Research Program of Frontier Sciences, CAS, China (QYZDYSSW-SLH021), and the Strategic Priority Research Program of Chinese Academy of Sciences (XDB25000000).

[1] S. Medvedev, T. M. McQueen, I. A. Troyan, T. Palasyuk, M. I. Eremets, R. J. Cava, S. Naghavi, F. Casper, V. Ksenofontov, G. Wortmann, and C. Felser, Nat. Mater. **8**, 630 (2009).

[2] Q.-Y. Wang, Z. Li, W.-H. Zhang, Z.-C. Zhang, J.-S. Zhang, W. Li, H. Ding, Y.-B. Ou, P. Deng, K. Chang, J. Wen, C.-L. Song, K. He, J.-F. Jia, S.-H. Ji, Y.-Y. Wang, L.-L. Wang, X. Chen, X.-C. Ma, and Q.-K. Xue, Chin. Phys. Lett. **29**, 037402 (2012).

[3] S. Tan, Y. Zhang, M. Xia, Z. Ye, F. Chen, X. Xie, R. Peng, D. Xu, Q. Fan, H. Xu, J. Jiang, T. Zhang, X. Lai, T. Xiang, J. Hu, B. Xie, and D. Feng, Nat. Mater. **12**, 634 (2013).

[4] S. He, J. He, W. Zhang, L. Zhao, D. Liu, X. Liu, D. Mou, Y. B. Ou, Q. Y. Wang, Z. Li, L. Wang, Y. Peng, Y. Liu, C. Chen, L. Yu, G. Liu, X. Dong, J. Zhang, C. Chen, Z. Xu *et al.*, Nat. Mater. **12**, 605 (2013).

[5] J. Guo, S. Jin, G. Wang, S. Wang, K. Zhu, T. Zhou, M. He, and X. Chen, Phys. Rev. B **82**, 180520(R) (2010).

[6] A. F. Wang, J. J. Ying, Y. J. Yan, R. H. Liu, X. G. Luo, Z. Y. Li, X. F. Wang, M. Zhang, G. J. Ye, P. Cheng, Z. J. Xiang, and X. H. Chen, Phys. Rev. B **83**, 060512(R) (2011).

[7] J. J. Ying, X. F. Wang, X. G. Luo, A. F. Wang, M. Zhang, Y. J. Yan, Z. J. Xiang, R. H. Liu, P. Cheng, G. J. Ye, and X. H. Chen, Phys. Rev. B **83**, 212502 (2011).

[8] X. F. Lu, N. Z. Wang, H. Wu, Y. P. Wu, D. Zhao, X. Z. Zeng, X. G. Luo, T. Wu, W. Bao, G. H. Zhang, F. Q. Huang, Q. Z. Huang, and X. H. Chen, Nat. Mater. **14**, 325 (2015).

[9] M. Z. Shi, N. Z. Wang, B. Lei, C. Shang, F. B. Meng, L. K. Ma, F. X. Zhang, D. Z. Kuang, and X. H. Chen, Phys. Rev. Materials **2**, 074801 (2018).

[10] M. Z. Shi, N. Z. Wang, B. Lei, J. J. Ying, C. S. Zhu, Z. L. Sun, J. H. Cui, F. B. Meng, C. Shang, L. K. Ma, and X. H. Chen, New J. Phys. **20**, 123007 (2018).

[11] B. L. Kang, M. Z. Shi, S. J. Li, H. H. Wang, Q. Zhang, D. Zhao, J. Li, D. W. Song, L. X. Zheng, L. P. Nie, T. Wu, and X. H. Chen, Phys. Rev. Lett. **125**, 097003 (2020).

[12] K. Ueno, H. Shimotani, H. Yuan, J. Ye, M. Kawasaki, and Y. Iwasa, J. Phys. Soc. Jpn. **83**, 032001 (2014).

[13] B. Lei, J. H. Cui, Z. J. Xiang, C. Shang, N. Z. Wang, G. J. Ye, X. G. Luo, T. Wu, Z. Sun, and X. H. Chen, Phys. Rev. Lett. **116**, 077002 (2016).

[14] B. Lei, N. Z. Wang, C. Shang, F. B. Meng, L. K. Ma, X. G. Luo, T. Wu, Z. Sun, Y. Wang, Z. Jiang, B. H. Mao, Z. Liu, Y. J. Yu, Y. B. Zhang, and X. H. Chen, Phys. Rev. B **95**, 020503(R) (2017).

[15] T. P. Ying, M. X. Wang, X. X. Wu, Z. Y. Zhao, Z. Z. Zhang, B. Q. Song, Y. C. Li, B. Lei, Q. Li, Y. Yu, E. J. Cheng, Z. H. An, Y. Zhang, X. Y. Jia, W. Yang, X. H. Chen, and S. Y. Li, Phys. Rev. Lett. **121**, 207003 (2018).

[16] L. Ma, B. Lei, N. Wang, K. Yang, D. Liu, F. Meng, C. Shang, Z. Sun, J. Cui, C. Zhu, T. Wu, Z. Sun, L. Zou, and X. Chen, Sci. Bull. **64**, 653 (2019).

[17] Y. Cui, G. Zhang, H. Li, H. Lin, X. Zhu, H.-H. Wen, G. Wang, J. Sun, M. Ma, Y. Li, D. Gong, T. Xie, Y. Gu, S. Li, H. Luo, P. Yu, and W. Yu, Sci. Bull. **63**, 11 (2018).

[18] Z. Li, S. Shen, Z. Tian, K. Hwangbo, M. Wang, Y. Wang, F. M. Bartram, L. He, Y. Lyu, Y. Dong, G. Wan, H. Li, N. Lu, J. Zang, H. Zhou, E. Arenholz, Q. He, L. Yang, W. Luo, and P. Yu, Nat. Commun. **11**, 184 (2020).

[19] G. Zheng, W. Q. Xie, S. Albarakati, M. Algarni, C. Tan, Y. Wang, J. Peng, J. Partridge, L. Farrar, J. Yi, Y. Xiong, M. Tian, Y. J. Zhao, and L. Wang, Phys. Rev. Lett. **125**, 047202 (2020).

[20] G. Zheng, M. Wang, X. Zhu, C. Tan, J. Wang, S. Albarakati, N. Aloufi, M. Algarni, L. Farrar, M. Wu, Y. Yao, M. Tian, J. Zhou, and L. Wang, Nat. Commun. **12**, 3639 (2021).

[21] Y. Cui, Z. Hu, J.-S. Zhang, W.-L. Ma, M.-W. Ma, Z. Ma, C. Wang, J.-Q. Yan, J.-P. Sun, J.-G. Cheng, S. Jia, Y. Li, J.-S. Wen, H.-C. Lei, P. Yu, W. Ji, and W.-Q. Yu, Chin. Phys. Lett. **36**, 077401 (2019).

[22] M. Jo, H. J. Lee, C. Oh, H. Yoon, J. Y. Jo, and J. Son, Adv. Funct. Mater. **28**, 1802003 (2018).

[23] See Supplemental Material at http://link.aps.org/supplemental/10.1103/PhysRevB.106.014509 for more details about the thickness of proton conductor film and transport properties of proton-intercalated FeSe thin flakes.

[24] B. Lei, Z. J. Xiang, X. F. Lu, N. Z. Wang, J. R. Chang, C. Shang, A. M. Zhang, Q. M. Zhang, X. G. Luo, T. Wu, Z. Sun, and X. H. Chen, Phys. Rev. B **93**, 060501(R) (2016).

[25] H. Lei, D. Graf, R. Hu, H. Ryu, E. S. Choi, S. W. Tozer, and C. Petrovic, Phys. Rev. B **85**, 094515 (2012).

[26] A. Subedi, L. Zhang, D. J. Singh, and M. H. Du, Phys. Rev. B **78**, 134514 (2008).

[27] T. Qian, X. P. Wang, W. C. Jin, P. Zhang, P. Richard, G. Xu, X. Dai, Z. Fang, J. G. Guo, X. L. Chen, and H. Ding, Phys. Rev. Lett. **106**, 187001 (2011).

[28] X. H. Niu, R. Peng, H. C. Xu, Y. J. Yan, J. Jiang, D. F. Xu, T. L. Yu, Q. Song, Z. C. Huang, Y. X. Wang, B. P. Xie, X. F. Lu, N. Z. Wang, X. H. Chen, Z. Sun, and D. L. Feng, Phys. Rev. B **92**, 060504(R) (2015).

[29] Y. Miyata, K. Nakayama, K. Sugawara, T. Sato, and T. Takahashi, Nat. Mater. **14**, 775 (2015).

[30] M. Khodas and A. V. Chubukov, Phys. Rev. Lett. **108**, 247003 (2012).

[31] E. M. Nica, R. Yu, and Q. Si, npj Quantum. Mater. **2**, 24 (2017).